A Communication Theoretical Modeling of Single-Walled Carbon Nanotube Optical Nanoreceivers and Broadcast Power Allocation

Burhan Gulbahar and Ozgur B. Akan, *Senior Member, IEEE*

***Abstract*—Carbon nanotube (CNT) with its ground-breaking properties is a promising candidate for future nanoscale communication networks. CNTs can be used as on-chip optical antenna for wireless interconnects. Carbon nanotube field-effect transistors (CNTFETs) show significant performance as photodetectors due to wide spectral region and tunable bandgap. In this paper, CNTFETs composed of semiconducting single-walled carbon nanotube (SWNT) and metal contacts (M-SWNT-M) are used as photodiode receivers in nanoscale optical communication by theoretically modeling diameter-dependent characteristics for shot-, dark-, and thermal-noise-limited cases. Bit error rate (BER), cutoff bit rate, and signal-to-noise ratio performance are analyzed for intensity modulation and direct detection modulation. The multireceiver CNT nanoscale network topology is presented for information broadcast and the minimum SNR is maximized solving NP-hard max–min power allocation problem with semidefinite programming relaxation and branch and bound framework. The significant performance improvement is observed compared with uniform power allocation. Derived model is compared with existing experiments and hundreds of Mb/s data rate is achievable with very low BERs. Furthermore, optimization gain is highest for thermal-noise-limited case while the shot-noise-limited case gives the highest data rate.**

***Index Terms*—Bit error rate (BER), broadcast, carbon nanotube (CNT), optical network, power allocation, signal-to-noise ratio (SNR).**

I. Introduction

CARBON nanotube (CNT) is a ground-breaking material discovered two decades ago with tremendous number of applications in physical and technological sciences including molecular electronics, quantum computing and nanoscale communications. Single-walled carbon nanotubes (SWNTs) as 1-D nanometer size strips of graphene are promising to be utilized in future nanonetworks due to fascinating mechanical, electrical, and thermal properties [1], [2].

Manuscript received July 25, 2011; accepted November 15, 2011. Date of publication November 29, 2011; date of current version March 9, 2012. This work was supported in part by the Turkish Scientific and Technical Research Council (TUBITAK) under Grant #109E257, by the Turkish National Academy of Sciences Distinguished Young Scientist Award Program (TUBA-GEBIP), and by IBM through IBM Faculty Award. The review of this paper was arranged by Associate Editor M. P. Anantram.

The authors are with the Next-generation and Wireless Communications Laboratory, Department of Electrical and Electronics Engineering, Koc University, Istanbul 34450, Turkey (e-mail: bgulbahar@ku.edu.tr; akan@ku.edu.tr).

Digital Object Identifier 10.1109/TNANO.2011.2177500

Carbon nanotube field-effect transistors (CNTFETs) competitive with the state-of-the-art silicon transistors are promising candidates for future nanoscale electronics [2]. Furthermore, with tunable bandgap, wide spectral range response and polarized absorption, SWNTs are efficient photodetectors in nanoscale optoelectronics. Moreover, Schottky barrier CNTFET photodiodes composed of semiconducting SWNT and metal contacts (M-SWNT-M) have a considerable quantum efficiency and very small dark currents [3]–[10]. Photodiodes built with CNT p-n junctions show current–voltage characteristics similar to conventional diodes [11]–[14]. SWNTs can be used as photovoltaic cells [10], [14]–[17]. These devices perform optical-to-electrical conversion and are strong candidates for nanoscale optoelectronics.

In addition, SWNTs are candidates in network-on-chip (NoC) platforms for future wireless interconnects as optical antennas. CNTs operate in terahertz and optical frequency range, have large bandwidth and perform as both transmitter and receiver with simple ON–OFF keying [18]–[21]. However, there is no theoretical modeling of performance characteristics, e.g., signal-to-noise ratio (SNR), bit error rate (BER) and achievable data rates, for a CNT nanoscale optical receiver. It is of fundamental importance to model the diameter-dependent performance, validate with existing experiments and discuss power allocation for a nanoscale optical network of receivers having performance differences due to diameter variation.

In this paper, for the first time, CNT receivers based on M-SWNT-M photodiodes with small diameter nanotubes, i.e., (0.7–1.2) nm, are modeled theoretically within an optical communication perspective. Photocurrent and noise modeling are combined to compute the diameter-dependent performance metrics, i.e., SNR, BER and cutoff bit rate or receiver data rate, i.e., R_b. The parameter fitting of the model with the experiments in literature is achieved. The performance is analyzed for intensity modulation and direct detection (IM/DD) nonreturn-to-zero ON–OFF keying modulation in shot-, dark-, and thermal-noise-limited (NL) cases. The multiuser CNT *ad hoc* network topology for information broadcast is presented and the maximization of the minimum SNR is modeled as an NP-hard quadratic power allocation problem among transmitter frequencies for dark- and thermal-NL cases. Linear programming (LP) and semidefinite programming relaxation (SDP) solutions combined with branch and bound (BB) framework, i.e., SDP-BB, are presented. Uniform power allocation (UPA) with practical transmit power levels results in hundreds of Mb/s data rate with very low BERs. Furthermore, optimum power allocation (OPA) gives significant

improvement in terms of SNR gain and R_b increasing with the diameter range. Thermal-NL case gives the highest gain, while shot-NL case gives the highest data rate.

The remainder of this paper is organized as the following. In Section II, the related work on CNT optical receivers is explored. In Section III, they are theoretically modeled, and in Section IV, optical transmitter models are discussed. Then, in Section V, multiuser broadcast for CNT nanoscale optical network topology is presented. In Section VI, max–min SNR problem is presented and the SDP-BB solution is given. In Section VII, after discussing parameter fitting of proposed model with existing experiments, cutoff data rates, and transmitter power levels, BER and SNR performances are analyzed. Max–min SNR is numerically evaluated and compared with UPA. Finally, in Section VIII, the conclusions are given.

II. Related Work

CNTs performing as optical antennas can achieve low-cost ultrafast computer technologies [22]. In [18]–[21], CNTs are offered as terahertz range on-chip nanoscale antennas. The advantages of wireless NoCs (WiNoC) in terms of throughput and large bandwidths of CNT optical antennas (500 GHz) are discussed. Antenna absorbance is shown to depend quadratically on the nanotube diameter and linearly on the conductivity. Furthermore, the time, frequency, and polarization division multiplexing (TDM, FDM, PDM) schemes are discussed [19]. However, in these studies, SWNT photodiodes are not analyzed in terms of SNR modeling, but a simplified nanoantenna concept is utilized. Power allocation discussion for CNT multiuser nanoscale optical networks is not available. SNR for dipole CNT antennas is discussed in [23], but networking and receiver modeling approaches are not presented.

CNT photodetectors are analyzed theoretically and experimentally in various works. CNTFET photodetectors perform optical-to-electrical conversion in [3]–[7]. Similarly, photodiode devices are formed of CNT p-n junctions in [11]–[13] or M-SWNT-M devices in [8]–[10], and [14]. Photovoltaic cells made of SWNTs are analyzed in [10], [14]–[17]. In these works, it is observed that it is possible to obtain efficient photocurrent conversion efficiencies and low dark currents making SWNT a candidate optical nanoreceiver. Although the SWNT photodiode devices are analyzed in great detail, their utilization in optical communications is not analyzed. Furthermore, SNR analysis for a CNTFET considering shot-, dark-, and thermal-NL cases is not available within an optical communications and networking perspective.

To the best of our knowledge, this is the first work analyzing CNT nanoscale optical communication networking with a detailed receiver modeling and numerical analysis of photocurrent spectrum, SNR, BER and R_b. Multichannel broadcast, multireceiver nanoscale optical network and optimization of transmitter power allocation are, for the first time, presented and analyzed. By applying UPA with practical transmit power levels, the feasibility of the information rate of hundreds of Mb/s with very small BERs, for the first time, is shown for CNT photodetectors. The transmit power allocation problem is, for the first time, modeled as a max–min quadratic optimization problem for dark- and thermal-NL cases and as an LP problem for shot-NL case, and solved with SDP-BB and LP algorithms. Uniform and optimum power allocations are compared and the significant performance improvement is observed for the broadcast network in terms of SNR gain and maximum R_b as a novel result.

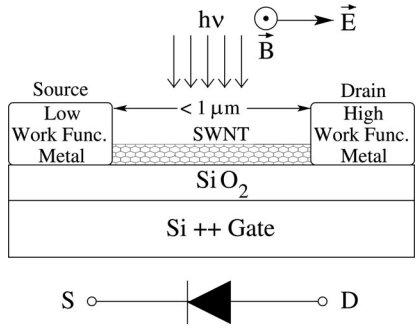

Fig. 1. Physical structure of an asymmetric M-SWNT-M photodiode, where the electric field of the optical signal is polarized along the NT axis [9], [10].

III. CNT Optical Receiver Model

CNTs are increasingly being used in various CNTFET photodetectors [3]–[7], photodiodes [11]–[14], [16], or M-SWNT-M devices [8]–[10]. These works are generally experimental and theoretical modeling of the receivers and networking basics are not available. In this paper, SWNT optical receiver is assumed to be of CNTFET photodiode type having better efficiencies compared with other experiments [9]. The physical structure of an asymmetric M-SWNT-M photodiode is shown in Fig. 1. It consists of two metals with different work functions connected to SWNT either suspended or on SiO_2 substrate and an Si back-gate managing Schottky barriers.

The modulation type is assumed to be of type IM/DD with nonreturn-to-zero ON–OFF keying [24] such that the information signal with bandwidth B modulates the instantaneous transmitted optical power at transmission frequency ν and the photocurrent being proportional to the received power carries the data signal. Next, the basic CNT optical photodiode receiver is analyzed and modeled in terms of its equivalent circuit, photocurrent, and SNR.

A. Equivalent Circuit Model

Photodiodes are described by their equivalent circuits to model noise sources and cutoff frequency, by evaluating the resistive and capacitive elements of the amplifier and photodiode itself. Then, SNR and R_b can be evaluated for IM/DD optical channel [24]. In this paper, M-SWNT-M photodiodes are used with asymmetrical contacts increasing the photocurrent performance compared with the symmetric ones and show a diode-like behavior [9]. Resistive Schottky barrier contact and ohmic contact are formed between SWNT and a low, e.g., Ti, and high, e.g., Pt, work function metal in source and drain electrodes, respectively. The reverse bias region is chosen to minimize dark current, i.e., I_d, and maximize photocurrent, i.e., I_p.

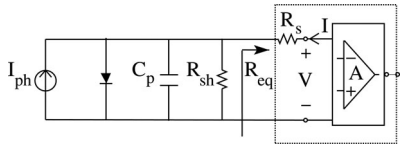

Fig. 2. Equivalent circuit of a CNT photodiode [16], [25].

CNT photodiode equivalent circuit is given in Fig. 2. The model is used for SWNT diode in [25] and p-n junction in [16]. I_p is modeled as a current source parallel to a diode and the shunt (junction) resistance $R_{\rm sh}$, and in series with resistance R_s of CNT and $R_{\rm eq}$ of CNT and amplifier combination. R_s is the sum of resistances of the contact, i.e., R_c, and nanotube [2], [26]. It changes with tube diameter d_t, contact metals, Schottky barrier height, i.e., $\Phi_{\rm SB}$, and the gate voltage [2], [25], [26]. R_c approaches the quantum limit of $\sim$10 KΩ depending on the contact length [26]. However, more theoretical results are required to model the diameter dependence and out of scope of this paper. Furthermore, ultrasonic nanowelding method and parallel array of nanotubes decrease R_c [15], [25] substantially. R_s is measured for M-SWNT-M between 400 KΩ and 120 MΩ [12], [14], [16], [25]. $R_{\rm sh}$ which is large compared with R_s is ignored, i.e., 1.1–35 GΩ [14], [16].

C_p is the equivalent capacitance found as 30 aF/μm in [25] and $\approx$50 aF/μm (neglecting the much larger quantum capacitance) [27] leading to terahertz range cutoff frequency. C_p is $\propto 1/\ln(h_s/d_t)$, where h_s is the separation between metal plate and the nanotube [27]. For h_s between 8 and 500 nm, e.g., oxide thickness is 8, 200, and 500 nm in [5], [9], and [14], respectively, C_p ratio of the 0.7 and 1.2 nm diameter tubes is between 0.78 and 0.92 and their capacitances can be assumed equal. Therefore, C_p is set to 30 aF/μm as in [25].

I_d depends on $\Phi_{\rm SB}$ and d_t (nm) [12], [25]. If Fermi-level pinning is not taken into account, Schottky barrier height of holes (assuming p-type CNT [25], [28]) at the source is given by $\Phi_{SB} = \Phi_{\rm CNT} - \Phi_M + E_g/2$, where $\Phi_{\rm CNT} \approx 4.9$ eV and Φ_M are the work functions of SWNT and the metal, respectively, and E_g is SWNT bandgap [2]. I_d is computed by using Thermionic Emission (TE) current as the following:

$$I_d = D_s \exp\left(-\frac{a_{CC}\gamma}{d_t \kappa T}\right) = D_s \exp\left(-\frac{15.78}{d_t}\right) \qquad (1)$$

where $D_s = AA^*T^2 \exp\left((\Phi_M - \Phi_{\rm CNT})/\kappa T\right)$, κ is the Boltzmann constant, T is the absolute temperature (thermal energy $\kappa T = 26$ meV), q is the electric charge, $A^* = (4\pi q m^* \kappa^2)/h^3$ is the Richardson constant, A is the contact area (assume a constant value for all nanotubes), m^* is the CNT effective mass, $a_{CC} = 0.142$ nm is the bond length, $\gamma = 2.89$ eV is the overlap integral, h is Planck's constant, and $E_g = 2a_{CC}\gamma/d_t$ [2], [26]. Small diameter tubes are chosen for obtaining small I_d.

Shockley diode equation for the circuit shown in Fig. 2 is given by $I = (V - IR_{\rm sh})/R_{\rm sh} + I_d(\exp(q(V - IR_s)/(n\kappa T)) - 1) - I_p$, where n is the ideality factor (1 to 2) [25]. In reverse bias of $V < 0$ and $R_{\rm sh} \gg 0$, $I = -I_d - I_p$, i.e., the sum of dark and photocurrent. Next, the diameter-dependent photocurrent is modeled.

B. Photocurrent Model

Optical communication channels convert the optical power to photocurrent signal [24]. Absorbed photons generate electron–hole (e-h) pairs that are separated and collected at the external circuit [2], [3]. In this study, IM/DD optical communication baseband channel is modeled as $I_r(t,\nu) = I_p(t,\nu) + n(t)$, where $I_r(t,\nu)$ is the receiver current at frequency ν, $I_p(t,\nu) = \mathcal{R}(t,\nu)P_t(t,\nu) * h(t) = \mathcal{R}(t,\nu)P_i(t,\nu)$, $\mathcal{R}(t,\nu)$ is the responsivity, $P_t(t,\nu)$ and $P_i(t,\nu)$ are the transmit and incident powers, respectively, $h(t)$ is the channel impulse response and $n(t)$ is the independent white Gaussian noise [24]. In this study, the modeling of the channel $h(t)$ and the power-loss analysis between the transmitter and the receiver is out of scope and a line-of-sight (LOS) link is assumed [24].

Carrier generation depends on the absorption coefficient $\alpha(\nu)$. Internal quantum efficiency of a photodetector, i.e., $\eta_{\rm In}(\nu) = I_p \hbar\nu/(qP_a(\nu))$, is defined as the ratio of the count of the absorbed photons to the generated carriers, where $P_a(\nu)$ is the absorbed power [3]. The maximum $\eta_{\rm In}$ at the peaks is almost diameter independent [11]. The peaks are at transition energies denoted with E_{ii} and $E_{ij}, i \neq j$, where $i, j = 1, 2, \ldots$, for light polarization parallel and perpendicular to the nanotube axis, respectively [29]. Semiconducting CNTs show strong absorption anisotropy [17], and the incident light is assumed to be polarized parallel as shown in Fig. 1. They are direct bandgap materials with diameter tunable E_{ii} making them efficient photodevices [29].

E_{ii} values are analyzed in excitonic picture [4]. Higher energy excitons create free e-h pairs by embedding in lower energy states. However, E_{11} excitons are difficult to dissociate due to large binding energies [29]. Therefore, photocurrent corresponding to E_{22} is considered, while the developed framework can be applied to E_{11}. Optical transition frequencies corresponding to $E_{ii} = h\nu_{ii}$ versus d_t shown in Fig. 3 are modeled by

$$E_{ii}(d_t) = a\frac{i}{d_t} + ab\frac{i}{d_t}\log\left(\frac{c}{i/d_t}\right) + \beta_i \frac{\cos 3\theta}{d_t^2} \qquad (2)$$

where $a = 1.049$ (eV nm), $b = 0.456$, $c = 0.812$ nm^{-1}, $\beta_i = \beta'_{i,p}$ for the tube with index (n,m), where $p = \text{mod}(2n + m, 3)$, $[\beta'_{1,1} \;\; \beta'_{1,2} \;\; \beta'_{2,1} \;\; \beta'_{2,2}] = [0.05 \;\; -0.07 \;\; -0.19 \;\; 0.14]$, $d_t = a_{CC}\sqrt{3(n^2 + nm + m^2)}/\pi$, and chiral angle $\theta = \tan^{-1}\left(\sqrt{3}m/(2n + m)\right)$ [2].

Nonequilibrium Green's function (NEGF) theoretical simulation shows that $\eta_{\rm In} \approx \%17$ [11] and $\approx \%58.97$ [10] for an asymmetric photovoltaic device. Experimentally, $\eta_{\rm In} > \%10$ for SWNT p-n junction [3] and the responsivity $\mathcal{R} = 2 \times 10^{-3}$ A/W [6] makes CNT photodiodes very efficient for nanoscale optical networks.

Photocurrent should be modeled in terms of ν and d_t dependence to compare different diameter CNTs. Absorption and photocurrent spectrum of CNTs are fitted by Lorentzian curves [3],

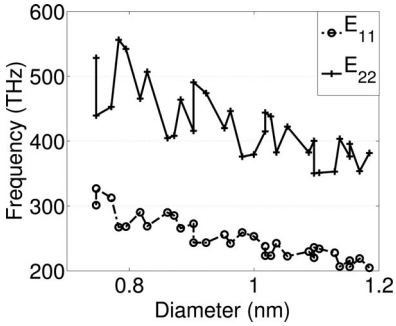

Fig. 3. Optical transition frequency versus semiconducting CNT diameter.

[4], [30]. The absorption spectra is represented as

$$\alpha_a(E) = \sum_{i=1}^{2} A_i \frac{\Gamma_{i,a}}{\pi\left(\Gamma_{i,a}^2 + (E - E_{ii})^2\right)} \tag{3}$$

where A_i is the absorption strength, $\Gamma_{i,a}$ is the linewidth, and $E = h\nu$. $A_i \propto d_t$ in a nonorthogonal tight-binding framework and follows a power-law behavior, i.e., $\propto 1/\sqrt{E_{ii}}$ [31]. Therefore, A_i can be modeled as $A_1 = C_2 d_t$ and $A_2 = A_1\sqrt{E_{11}/E_{22}}$.

Furthermore, it can be assumed that $P_a(\nu)$ is linearly proportional to the frequency (ω) dependent imaginary part of SWNT dielectric function ($\varepsilon_i(\omega)$) by treating them as lossy dielectric cylinders [3], [17]. By using $\alpha_a = \varepsilon_i(\omega)\omega/(n_d c)$, where n_d is the refractive index [32] and c is the speed of light and assuming $P_a(\nu)$ depends linearly on d_t^2 [17] and length L, $P_a(\nu)$ can be approximated as

$$P_a(\nu) = \Upsilon_1\sqrt{\frac{\nu_{11}}{\nu_{22}}}\frac{d_t^3 L P_i(\nu) B_l}{\pi h^2 \nu\left(B_l^2 + 4(\nu - \nu_{22})^2\right)} \tag{4}$$

where $B_l = \Gamma_{2,\mathrm{ph}}/h$, Υ_1 is a global normalization constant, and $\Gamma_{2,\mathrm{ph}}$ is the photocurrent Lorentzian bandwidth with values of 90–100 meV [3]–[5], [12]. Therefore, $\Gamma_{2,\mathrm{ph}}$ is set to 100 meV. Total photocurrent is given by $I_p = \int_{\nu_{\min}}^{\nu_{\max}} q\eta_{\mathrm{In}}(\nu)\left(P_a(\nu)/(h\nu)\right)d\nu$, where $P_i(\nu)$ (W/Hz) is the transmit optical power density and the total incident power is $P_{\mathrm{tot}} = \int_{\nu_{\min}}^{\nu_{\max}} P_i(\nu)d\nu$. Therefore, combining with (4), I_p is given by

$$I_p = \Upsilon_2\sqrt{\frac{\nu_{11}}{\nu_{22}}}d_t^3\int_{\nu_{\min}}^{\nu_{\max}}\frac{P_i(\nu)}{\nu^2\left(B_l^2 + 4(\nu - \nu_{22})^2\right)}d\nu \tag{5}$$

where $B_l = 24.18$ THz, $\Upsilon_2 = \Upsilon_1 q\eta_{\mathrm{In}} B_l L/(\pi h^3)$ is a constant. Next, the noise is modeled and SNR is computed.

C. Noise Model and SNR

Three dominant types of photodiode noise are *thermal noise* due to interaction between electrons and vibrating ions, *shot noise* caused by dark current and incident photons due to fluctuations of the discrete carriers [24] and low-frequency $1/f$ noise [33]. There is no theoretical modeling and experimental validation of SNR calculation for an SWNT photodiode.

CNT shot noise depends on *Fano factor*, i.e., $\mathcal{F}$, suppressing the noise compared with the conventional bulk semiconductors [34]. $1/f$ noise is neglected due to the assumption of operating frequencies higher than 1 kHz [33]. The noise spectral densities of thermal and shot noise components can be described by $\sigma_t = 4\kappa T/R_{\mathrm{eq}}$ where $\kappa = 1.38\times10^{-23}$ J/K, $T = 300$ K (room temperature), and $\sigma_{\mathrm{Shot}} = \sigma_s + \sigma_d = 2qI_p + \mathcal{F}2qI_d$ where $0 < \mathcal{F} \leq 1$ and $q = 1.602\times10^{-19}$ C. Depending on R_{eq} and the comparison of σ_{Shot} and σ_t, three different NL operating regimes are defined as the following.

1) Shot NL, if $\sigma_t \ll \sigma_{\mathrm{Shot}} \approx 2qI_p$ s.t. $I_p \gg I_d$
2) Dark NL, if $\sigma_t \ll \sigma_{\mathrm{Shot}} \approx \mathcal{F}2qI_d$ s.t. $I_d > I_p$
3) Thermal NL, if $\sigma_{\mathrm{Shot}} \ll \sigma_t$ s.t. $R_s \leq R_{\mathrm{eq}}$.

Therefore, using I_d and assuming η_{In} is constant, SNR, i.e., $\gamma(d_t) = I_p^2/(\sigma B)$, for the shot-, dark-, and thermal-NL cases, i.e., γ_s, γ_d, and γ_t, respectively, are given by

$$\gamma_s(d_t) = h_s(d_t)\int_{\nu_{\min}}^{\nu_{\max}}\frac{P_i(\nu)}{\nu^2\left(B_l^2 + 4(\nu - \nu_{22})^2\right)}d\nu \tag{6}$$

$$\gamma_{d,t}(d_t) = h_{d,t}(d_t)\left(\int_{\nu_{\min}}^{\nu_{\max}}\frac{P_i(\nu)}{\nu^2\left(B_l^2 + 4(\nu - \nu_{22})^2\right)}d\nu\right)^2 \tag{7}$$

where the subscript s denotes shot-NL case, subscript (d,t) denotes dark- and thermal-NL cases, and

$$h_s(d_t) = \frac{\Upsilon_2}{2qB}\sqrt{\frac{\nu_{11}}{\nu_{22}}}d_t^3 \tag{8}$$

$$h_d(d_t) = \frac{\Upsilon_2^2}{2q\mathcal{F}D_s B}\frac{\nu_{11}}{\nu_{22}}d_t^6\exp\left(\frac{15.78}{d_t}\right) \tag{9}$$

$$h_t(d_t) = \frac{\Upsilon_2^2}{4\kappa T B}\frac{\nu_{11}}{\nu_{22}}d_t^6 R_{\mathrm{eq}}. \tag{10}$$

Except the shot-NL case, all the SNRs depend on the square of the input power. Next, the modeled SNRs are used in a multireceiver nanoscale optical network.

IV. Optical Transmitter Model

In this paper, theoretically modeled CNT photodetector receivers are based on the experimental works [3], [4], [6], [8], [9], [12], [35] carried out with commercially available transmitting laser sources, i.e., near-IR laser with a wavelength of 830 nm and power of ≈6 W/mm^2 with spot size around 200 μm [9], [35], continuous wave (CW) Ti/Sapphire laser tunable between 780–980 nm [3] and 720–1000 nm [4] with incident power around 10 W/mm^2, and Ti/Sapphire laser with spot size of 2 μm [6]. Furthermore, similar experiments are carried out for graphene photodetectors [36] with Agilent Lightwave Component Analyzers, i.e., N4375B and N4373C, with built-in 1550-nm lasers with the light intensity modulation frequencies available up to 67 GHz.

Although experimentally validated macroscale laser sources can be used to send information to nanoscale receivers, nanoscale optical transmitter devices, e.g., highly efficient light-emitting sources using CNT p-n diodes [37], low-power

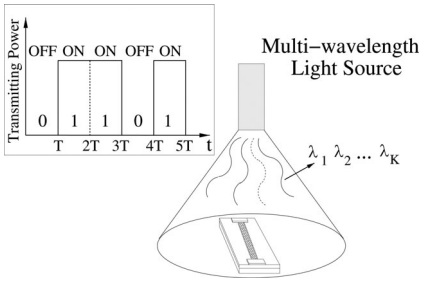

Fig. 4. Multiwavelength light source transmitting intensity modulated signal on CNT receiver. The inset shows an illustrative ON–OFF keyed data pattern modulating the intensity of the light.

dissipating nanoscale lasers reaching 100 GHz modulations, pW to nW radiation powers with ≈1 nm linewidths at room temperature [38], CNT optical antennas [21], [39], [40], can also be used for designing future nanoscale communication networks where both the transmitter and the receiver are formed of nanoscale devices. However, experimental works obtaining the light modulation of nanoscale transmitters using CNT or other technologies, the detection on CNT receivers for the light generated from these nanoscale light sources, and the theoretical modeling of the nanoscale transmitters in terms of power radiation are necessary to formulate the nanoscale transmitter–receiver communication channel. The design of the transmitter and the modeling of the power loss in the channel between receiver and the transmitter are out of scope of this paper. The receiver model is theoretically developed based on the amount of the incident power on CNT. Therefore, any transmitter device capable of generating optically modulated line-of-sight incident light density of the order of 0.5 mW/mm^2 or larger can be used as the transmitter unit such that 1 Kb/s or more data rate is possible as will be described in the simulations section.

Furthermore, the communication medium is the air or free space at room temperature as in experiments forming the basis for the nanoscale receiver models in this paper [8], [12] and conventional photodetector experiments [24]. Moreover, since CNT receivers are capable of absorbing light on continuous frequency bands with different central frequencies, and broadcast optimization is considered in this paper, either light sources capable of producing multifrequency light [41], [42] are needed to broadcast information simultaneously at multiple frequencies or tunable multiple light sources are utilized to broadcast information at various frequencies. However, the physical mechanism and the design of the transmitter light sources are out of scope of this paper. The transmitter and the receiver network scheme is shown in Fig. 4.

V. Multiple CNT Receiver Networking Topology

In this paper, different diameter CNT photodiodes are assumed to form a nanoscale *ad hoc* network distributed randomly in a nanoscale communication topology. Diameter variation is either realized intentionally to form heterogeneous receivers operating at different frequencies or as a result of the synthesis process, e.g., chemical vapor decomposition growths of nanotubes with Gaussian distributed diameters and uniformly distributed chiral angles [43].

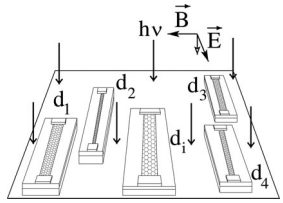

Fig. 5. Multireceiver broadcast nanoscale optical network topology of different diameter tubes.

The broadcast channel is important in nanoscale wireless networks where it is difficult to separately interact with individual units in a distributed nanonetwork [44], e.g., to direct the optical power to a single specific CNT receiver. For example, it could be very difficult to find the exact location of the receiver units in a network composed of receivers with different diameter nanotubes and to send specific wavelength light to specific position for a nanotube. Therefore, it is important to introduce and model the broadcast network. The broadcast nanoscale optical network is shown in Fig. 5.

Next, the broadcast power allocation optimization for CNT nanoscale optical network topology is presented.

VI. SNR Optimization Problem

The broadcast transmission power allocation specifies the minimum SNR of the weakest link, determining the maximum data rate in wireless networks [45]. Therefore, in a CNT *ad hoc* network with a finite amount of transmit power that can occur in future nanoscale optical communication scenarios, it is of uttermost importance to optimize power allocation. This is a max–min type optimization and analyzed for wireless networks as a downlink transmit beamforming in [45] and as multicast beamforming in [46].

The transmit optical power is assumed to be constant in finite intervals of frequencies, i.e., $\Delta\nu$, assuming that the total frequency spectrum is divided into intervals of $\Delta\nu$. Therefore, after some manipulations and calculating the indefinite integral, the integral equation for the photocurrent I_p in (6) and (7) can be represented as follows:

$$\int_{\nu_{\min}}^{\nu_{\max}} \frac{P_i(\nu)}{\nu^2\left(B_l^2+4\left(\nu-\nu_{22}\right)^2\right)}d\nu = \sum_{j=k_{\min}}^{k_{\max}} P_i(j\Delta\nu)f(j,d_t) \tag{11}$$

where $f(j,d_t)$ is the following:

$$f(j,d_t) = \frac{1}{j(j+1)\Delta\nu\left(4\nu_{22}^2+B_l^2\right)} + \frac{4\nu_{22}}{\left(4\nu_{22}^2+B_l^2\right)^2}\ln\left(\frac{B_l^2+4\varsigma^2(j)}{B_l^2+4\varsigma^2(j+1)}\frac{(j+1)^2}{j^2}\right) + 2\frac{4\nu_{22}^2-B_l^2}{B_l(4\nu_{22}^2+B_l^2)^2}\tan^{-1}\left(\frac{2\Delta\nu B_l}{B_l^2+4\varsigma(j)\varsigma(j+1)}\right) \tag{12}$$

and $\varsigma(j) = j\Delta\nu - \nu_{22}$. Then, SNR equations in (6) and (7) are transformed into the following:

$$\gamma_s(d_t) = \mathbf{p}^T \mathbf{a_s}(d_t), \quad \gamma_{d,t}(d_t) = \mathbf{p}^T \mathbf{A_{d,t}}(d_t)\mathbf{p} \tag{13}$$

where $\mathbf{p} = [P_i\,(k_{\min}\Delta\nu) \dots P_i\,(k_{\max}\Delta\nu)]^T$ represents the transmitter power densities at various frequencies and $\mathbf{A_{d,t}} \equiv h_{d,t}(d_t)\mathbf{f}(d_t)\mathbf{f}^T(d_t)$, $\mathbf{a_s} \equiv h_s(d_t)\mathbf{f}(d_t)$, and $\mathbf{f}(d_t) = [f(k_{\min}, d_t) \dots f(k_{\max}, d_t)]^T$.

Then, for the broadcast allocating the transmitter power among K optical frequencies, the optimization problems maximizing the minimum SNR among N nanotubes in the receiver network can be defined as max–min type problems such that

$$\max_{\mathbf{p}\in\mathbb{R}^{\mathbf{K}}} \min_{i=1,2,\dots,N} \mathbf{p}^T \mathbf{a_s}(d_i) \tag{14}$$

$$\max_{\mathbf{p}\in\mathbb{R}^{\mathbf{K}}} \min_{i=1,2,\dots,N} \mathbf{p}^T \mathbf{A_{d,t}}(d_i)\mathbf{p} \tag{15}$$

$$\text{s.t. } \mathbf{p}^T\mathbf{1} = P_{\max}, \quad \mathbf{p} \geq 0$$

where the subscript s denotes shot-NL case, subscript (d,t) denotes dark- and thermal-NL cases, respectively, $\mathbf{1_K}$ is the vector of length $K = k_{\max} - k_{\min} + 1$ (the number of distinct frequencies) with all ones, the total power is restricted to P_{tot} with total maximum density $P_{\max} = P_{\text{tot}}/\Delta\nu$, and the minimum SNR value among all N nanotubes is maximized with respect to $\mathbf{p}$.

For shot-NL case, (14) is converted to the following:

$$\min \mathbf{c}_{\text{LP}}^T\mathbf{x} \text{ s.t. } \mathbf{A}_{\text{LP}}\mathbf{x} = \mathbf{b}_{\text{LP}}, \quad \mathbf{x} \geq \mathbf{0} \tag{16}$$

$$\mathbf{x} = \begin{bmatrix} u \\ \mathbf{p} \\ \mathbf{s} \end{bmatrix}, \quad \mathbf{A}_{\text{LP}} = \left[\begin{array}{c|c|c} & -\mathbf{a_s^T}(d_1) & \\ \mathbf{1_N} & \vdots & \mathbf{I_N} \\ & -\mathbf{a_s^T}(d_N) & \\ \hline 0 & \mathbf{1}_{\mathbf{K}}^T & \mathbf{0}_{\mathbf{N}}^T \end{array}\right]$$

which is LP type and where $\mathbf{s} = [s_1 s_2 \dots s_N]^T$ is the column vector of slack variables, $\mathbf{c}_{\text{LP}} = \left[-1\ \mathbf{0}_{\mathbf{K}}^T\ \mathbf{0}_{\mathbf{N}}^T\right]$, $\mathbf{b}_{\text{LP}} = \left[\mathbf{0}_{\mathbf{N}}^T\ P_{\max}\right]$ and $\mathbf{I_k}$ is the unit vector of size k. Equation (16) is solved with Linear Interior Point Solver implemented under MATLAB environment [47].

For dark- and thermal-NL cases, (15) is transformed into

$$\max_{\mathbf{p}\in\mathbb{R}^{\mathbf{K}}, \mathbf{u}\in\mathbb{R}} u \quad \text{s.t.} \quad \mathbf{p}^T \mathbf{A_{d,t}}(d_i)\mathbf{p} \geq u, \mathbf{p}^T\mathbf{1} = P_{\max} \tag{17}$$

where $\mathbf{p} \geq 0$ and $i \in [1, N]$. This problem is a multiobjective extension of standard quadratic problem (StQP), where finding the global solution is NP hard [48]. However, a bound can be found by using SDP relaxation by converting the problem to the following [48]:

$$\max_{\mathbf{p}\in\mathbb{R}^{\mathbf{K}}} \min_{i=1,2,\dots,N} \text{Tr}(\mathbf{A_{d,t}}(d_i)\mathbf{P})$$

$$\text{s.t. Tr}(\mathbf{EP}) = P_{\max}^2, \quad \mathbf{p} \geq 0, \quad \mathbf{P} = \mathbf{p}\mathbf{p}^T \tag{18}$$

where $\mathbf{E}$ is the matrix of all ones. In an SDP problem, the symmetric structure of $\mathbf{P}$ and $\mathbf{p} \geq 0$ are replaced with constraints $\mathbf{P} \geq 0$ and $\mathbf{P}$ being symmetric positive semidefinite matrix, i.e., $\mathbf{P} \succeq 0$. This problem is solved efficiently in polynomial time using freely available toolboxes implemented in MATLAB, i.e., SeDuMi (IP methods) and CVX (for solving convex problems) [49], [50]. After finding the global solution $\mathbf{P}^*$, the feasible solution $\mathbf{p}^*$ is extracted by $\mathbf{p}_k^* = \alpha\sqrt{\mathbf{P}_{kk}^*}, k \in [1, K]$, with a scaling variable α to satisfy the total power constraint.

Algorithm 1: SDP-BB Algorithm

Solve the SDP relaxation in (18) and obtain $\mathbf{p}^* = ([p_1^*\, p_2^* \dots p_K^*])^T$
Set lower and upper bounds for each p_k, $B_{k,l} = \beta_{k,l}\, p_k^*$, $B_{k,u} = \beta_{k,u}\, p_k^*$
Order p_k from highest to lowest and form $K_{ord} = \{k_1, k_2, \dots, k_K\}$
for all $j = 1$ to K **do**
  Solve (19) for each $m \in [1, K_{sub}]$ finding the solution $SDP_{k_j,m}$
  Find $m = m_{k_j}^{max}$ where $SDP_{k_j,m}$ is highest and set $B_{k_j,l}$, $B_{k_j,u}$
end for
Solve the SDP relaxation in (18) with constraints $B_{k,l}$, $B_{k,u}$ and obtain final $\mathbf{p}_{opt}^*$

Besides that, max–min SNR beamforming frameworks in literature use randomization algorithms to better extract the complex valued solutions after finding the initial SDP relaxation solution $\mathbf{p}^*$ [45], [46]. Since the power is real valued in (17), the randomization algorithms cannot be applied and they are replaced with branch and bound search [51] by dividing the hyperplane $\mathbf{p}^T\mathbf{1} = P_{\max}$ into $K_{\text{sub}} = (\beta_{k,u} - \beta_{k,l})p_k^*/\Delta p_k$ regions for each k around the initial SDP bound $\mathbf{p}^*$ for constants K_{sub}, $\beta_{k,l} \leq 1$ and $\beta_{k,u} \geq 1$. K_{sub} increases the solution accuracy. The SDP-BB algorithm is given in Algorithm 1. The indices $k \in [1, K]$ are ordered with respect to the values of p_k^* from the highest to the lowest, i.e., $K_{ord} = \{k_1, k_2, \dots, k_K\}$, so that first the one with the maximum initial power is searched in order to more quickly converge to the optimum solution. Starting with $k = k_1$, SDP relaxations in (18) are solved with the additional constraint of $S_{k,m-1}^2 \leq P_{kk} \leq S_{k,m}^2$ for each $m \in [1, K_{\text{sub}}]$ where $S_{k,m} \equiv \beta_{k,l}p_k^* + m\Delta p_k$. After finding the maximum SDP bound for p_{k_j}, the corresponding optimum subinterval index ($m_{k_j}^{\max}$) is saved to be used in the next coming relaxations of $p_{k_{j+1}}, p_{k_{j+2}}, \dots, p_{k_K}$ for specifying the constraint for p_{k_j}. Therefore, SDP problem for the k_jth component at the mth subinterval can be expressed as

$$\max_{\mathbf{P}\geq 0, \mathbf{P}\geq 0} \min_{i=1,2,\dots,N} \text{Tr}(\mathbf{A_{d,t}}(d_i)\mathbf{P})$$

$$\text{s.t. Trace}(\mathbf{MP}) = P_M, S_{k_j,m-1}^2 \leq P_{k_jk_j} \leq S_{k_j,m}^2 \tag{19}$$

where $B_{k_n,l}^2 \leq P_{k_nk_n} \leq B_{k_n,u}^2$, $B_{k_n,l} = S_{k_n,m_{k_n}^{\max}-1}$, $B_{k_n,u} = S_{k_n,m_{k_n}^{\max}}$, and $n \in [1, j-1]$. $\mathbf{M}$ can be chosen as either $\mathbf{E}$ or $\mathbf{I}$, i.e., $P_M = P_E = P_{\max}^2$ or $P_M = P_I = P_{\max}$, choosing the hyperplane or quadratic constraint, respectively. Since the solution is scaled, either of the constraints can be used freely. The resulting K_{sub} bounds are compared and $m_{k_j}^{\max}$ giving the highest bound is chosen. Finally, (18) is solved with the constraint $B_{k,l}^2 \leq P_{kk} \leq B_{k,u}^2, k \in [1, K]$.

VII. Numerical Analysis

In simulations, it is assumed that the diameter range for the CNT network is $(d_c - \Delta d, d_c + \Delta d)$ for varying Δd, where $d_c = 0.95$ is chosen as the average of the small diameter range (0.7–1.2). SDP-BB parameters are chosen as $\beta_{k,l} = 0.2$ and $\beta_{k,u} = 4$, and the power is allocated for the spectrum between 300–700 THz with frequency interval of $\Delta\nu = 10$ THz,

TABLE I
REFERENCE M-SWNT-M DEVICE PERFORMANCES

d (nm)	λ (nm)	P_i (W/mm^2)	I_d (pA)	I_p (nA)	Source
1.4	830	$\approx$ 5.65	0.5	1	[9]
0.9	1127	1	-	0.043	[10]
2.6, 3	-	-	10, 500	-	[28]

d (nm)	I_d (pA)	Source
1.5, 1.76, 1.9	0.82, 2.92, 7.98	[12]

where the transmitted power is assumed to be constant. The wide spectral region covers absorption range of all the tubes with small diameter range $(0.7, 1.2)$, i.e., $\nu_{22}^{\min} \approx 350$ THz and $\nu_{22}^{\max} \approx 550$ THz. The performance of the CNT receivers is simulated assuming the receivers are of the same type with equal device structures but having different diameters.

First, photocurrent and dark current models in (5) and (1) are fit to experimental and theoretical works. Then, cutoff data rates and transmitter power levels are examined. Moreover, SNR and BER characteristics are analyzed for broadcast network and single receiver performance with UPA. Finally, uniform and optimum power allocations are compared for varying Δd.

A. Parameter Fitting for the Proposed Current Models

For numerical calculation of SNR and BER, the diameter-dependent photocurrent modeling in (5) and dark current in (1) are fit with experimental results and theoretical NEGF formalisms. For the experiments of asymmetrically contacted M-SWNT-M photodetectors, i.e., with Ag/Au [9] and Al/Au source–drain metal contacts [28], with SWNT Schottky barrier contact p-n diode [12] and for the theoretical asymmetrical M-SWNT-M photovoltaic device in [10] (corresponding to E_{11}) with Al/Au metal contacts, the obtained values given in Table I are used to derive approximate values for D_s and Υ_2 to be used in simulation studies in this paper.

D_s and Υ_2 are utilized by assuming the receivers have the same properties, e.g., device geometry, metal types, and back gate voltages, but different diameters. By inserting the values in Table I to (5) and (1), Υ_2 of 0.127 and 0.184 (A THz^4/nm pW) for [9] and [10], respectively, and D_s of 39.4 nA for [9], between 4.33 and 96.36 nA for [28] and between 23.15 and 32.35 nA for [12] are obtained. D_s values of different experiments give results in nanoampere range. Taking the experiment in [9], $D_s = 39.4$ nA and $\Upsilon_2 = 0.127$ (A THz^4/nm pW) are used in simulations. However, since I_d is very low, I_p needs to be very small to satisfy dark-NL regime and D_s is chosen larger to get larger SNR; $D_s = 96.36$ nA in [28] is used in this regime. Furthermore, *Fano factor* is set to 1 to realize the worst case dark noise contribution.

B. Cutoff Data Rate Computation

The cutoff rate, i.e., $f_c \geq B \approx R_b$, of photodetector receivers can be computed by using their transit time limited response times and calculating their *RC* limited bandwidths [24]. In this paper, cutoff rate of CNT detectors are computed by using the experimental measurements of the generated carriers of a recent work in [52] showing picoseconds (ps) time delay in CNT photocurrent measurements. The transit time ($t_{\rm tr}$) limited bandwidth is found by using the delay of the generated carriers in the nanotube to reach the metallic contacts, i.e., $f_c = 3.5/2\pi t_{\rm tr}$ [36]. Since the length of nanotubes is $L \leq 1$ μm, the group velocity of the carriers is $\approx 10^6$ m/s and carrier lifetime is ≈ 0.25 ns [52], it is computed that $t_{\rm tr} \approx 0.5$ ps and $f_c \approx 1.1$ THz. On the other hand, *RC* limited bandwidth, i.e., $1/2\pi R_{\rm eq} C_p$, is smaller than terahertz ranges and determines the resulting bandwidth for the equivalent capacitance $C_p = 30$ aF/μm of the devices. Even the ballistic limit $R_{\rm eq} = 10$ KΩ of nanotubes leads to $f_c = 1/2\pi R_{\rm eq} C_p \approx 0.5$ THz. Therefore, in various NL regimes, *RC* limited bandwidth decides the maximum data rate that the receiver can detect.

C. Transmitter Power Level

In simulation studies, two types of incident power levels are used. For calculation of the performance of single nanotubes, a wide range of power levels are simulated to observe BER characteristics under very small and very large power levels in the next section. On the other hand, for comparison of uniform and optimum power allocation schemes in a broadcast network and for observing the practical broadcast data rates, power transmitted along the linewidth $B_l = 24.18$ THz of a single tube is assumed to be in the experimentally available laser incident power range of 5–10 W/mm^2 [4], [9] for shot- and thermal-NL cases. For dark-NL case, the maximum power satisfying $I_p \ll I_d$ is found. In comparing I_p with I_d, and σ_t with $\sigma_{\rm Shot}$, ten times or more larger parameter is assumed to be the dominating one. Assuming that experimental laser incident power density of 5 W/mm^2 is applied at a single frequency for shot- and thermal-NL cases, the total transmitted incident power density, i.e., $P_{\rm tot,0}$, becomes $5 \times (700 - 300)/B_l \approx 82.7$ (W/mm^2) where $(700 - 300)/B_l$ is used to find the maximum number of absorption windows since each nanotube is assumed to absorb most of the light in B_l linewidth. For dark-NL case, maximum $P_{\rm tot,0} \approx 170$ (nW/ mm^2) incident power satisfies $I_p \ll I_d$ for the nanotubes. It is assumed that broadcast incident power level is $P_{\rm tot,0}$. Therefore, for $P_{\rm tot,0}$ incident power level, the power density per area and per Hertz for thermal- and shot-NL cases is given by $P_{\rm dens,0} = 82.7/400 \approx 0.2068$ (pW/mm^2 Hz) and for dark-NL case $P_{\rm dens,0} \approx 0.5 \times 170/400 \approx 0.2125$ (nW/mm^2 THz).

D. UPA BER and SNR Performance

For the power level of $P_{\rm tot,0}$ with UPA, $R_{\rm eq} \geq 285$ MΩ, $\leq$333 KΩ and $\geq$161 TΩ with fixed values along the network result in shot-, thermal-, and dark-NL cases, respectively, for all the tubes in the diameter range (0.7–1.2) nm. The threshold resistance values are chosen to simulate NL types. *RC* bandwidths of $f_c^{\rm dark} = 32$ Hz, $f_c^{\rm shot} = 18.6$ MHz, and $f_c^{\rm therm} = 15.93$ GHz are calculated for these specific resistances. Although $1/f$ noise is high and SNR is very low in dark-NL case, SNR is calculated to observe the diameter dependence. Next, BER and SNR are computed for both broadcast network and single receivers with UPA.

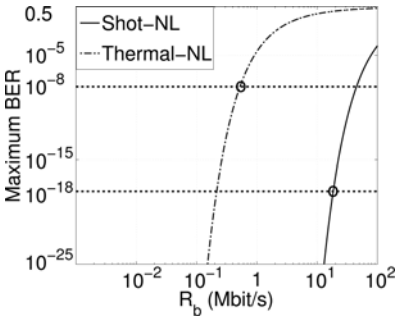

Fig. 6. BER of the worst performance tube versus broadcast R_b for UPA.

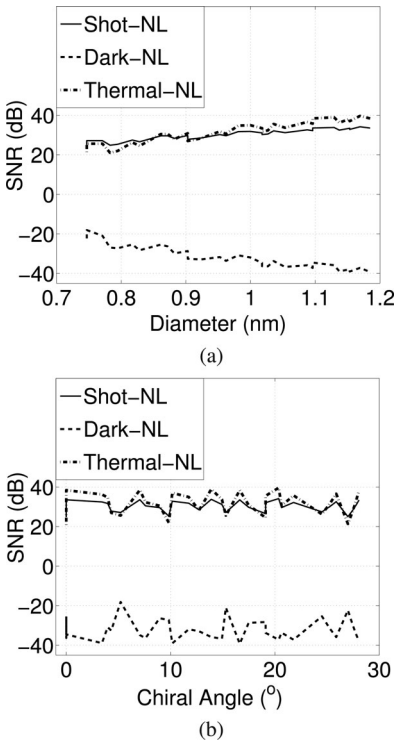

Fig. 7. SNR versus (a) the diameter d_t and (b) the chiral angle of single CNT receiver for UPA.

1) Broadcast Network: BERs of IM/DD nonreturn-to-zero ON–OFF keying modulation schemes are found by using the complementary error function, i.e., $\text{erfc}(x) = 2/\sqrt{\pi}\int_x^\infty e^{-x^2}dx$, with $\text{BER} = Q(\sqrt{\text{SNR}}/2)$, where $Q(x) = 0.5\ \text{erfc}(x/\sqrt{2})$ [53]. In Fig. 6, the BER of the worst performance tube in the network (all the tubes in the diameter range (0.7–1.2) nm) is shown for varying broadcast data rates R_b and the power level $P_{\text{tot},0}$. Assuming a BER threshold of 10^{-8} for Mb/s communication, $R_{b,s} < 44.9$ Mb/s and $R_{b,t} < 521$ Kb/s are found for shot- and thermal-NL cases, respectively. Since the cutoff frequency is smaller than the computed rate, i.e., $f_{c,1} < 44.9$ Mb/s, the maximum data rate satisfying BER is chosen as $R_{b,1} = f_{c,1} = 18.6$ MHz leading to a maximum BER of $\approx 10^{-18}$. The diameter and chiral angle dependence of SNR for the receivers in the broadcast network are shown in Fig. 7(a) and (b). There is an $\approx 9, 18$, and 21 dB difference, i.e., $\text{SNR}_r \equiv \text{SNR}_{\max}/\text{SNR}_{\min}$, between the maximum and minimum SNR among the tubes for shot-, thermal-, and dark-NL cases, respectively, as the diameter changes. SNR increases with respect to diameter for shot- and thermal-NL cases and decreases for dark-NL case. There is not an observable linear dependence on chiral angle. These observations, especially the oscillations, prove the distinct nature of nanotubes, which are due to the nonuniform optical transition energies, i.e., E_{ii}, with respect to the diameter and its effect in absorption and photocurrent in (4) and (5), and should be tested with experimental works.

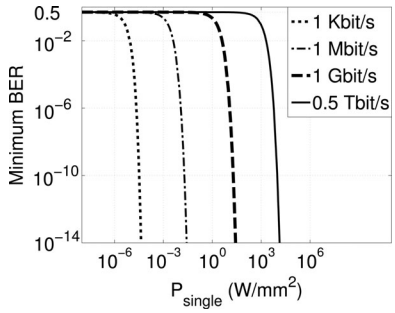

Fig. 8. Minimum BER among all the tubes versus P_{single} for varying R_b.

2) Single Receiver: The BER of the best performance tube, i.e., minimum BER along the network, is computed without considering NL cases but the total receiver noise, i.e., $\sigma_{\text{tot}} = \sigma_{\text{Shot}} + \sigma_t$, for varying R_b is shown in Fig. 8, where tubes are assumed to have adaptive and distinct R_{eq} such that the maximum rates and the BER performances of each tube are computed for a wide range of equivalent resistance values. The BER performance is plotted against the absorbed power per nanotube approximating the total absorbed power by finding the total power inside the absorption linewidth B_l, i.e., P_{single}. As the resistance value is lowered, the thermal noise component increases lowering the SNR. However, *RC* limited bandwidth increases allowing higher cutoff data rates. Therefore, the wide range of resistance values are simulated to find the maximum allowable data rate for a specific power level, BER threshold, and for all diameter nanotubes. For various combinations of R_b and power levels, the tube with the minimum BER is chosen.

BER of 10^{-6} is possible even with very low total incident power levels of $P_{\text{single}} \approx 20\ \mu\text{W/mm}^2$ at the minimum simulated communication rate $R_b = 1$ Kb/s. The maximum R_b is set to ≈ 0.5 THz, since the ballistic limit $R_{\text{eq}} = 10\ \text{K}\Omega$ leads to $f_c = 1/2\pi R_{\text{eq}} C_p \approx 0.5$ THz. It is observed that for 500 Gb/s communication link with BER lower than 10^{-14}, the nanotube should be feed with the incident optical power larger than $\approx 15\ \text{kW/mm}^2$ which is out of practical ranges. However, it is possible to achieve hundreds of Mb/s data for tens of W/mm^2 incident power density, e.g., BER of $\approx 10^{-11}$ at $R_b = 1$ Gb/s with power density of $\approx 20\ \text{W/mm}^2$. Next, OPA and UPA are compared for varying Δd in a broadcast optical nanonetwork.

E. Optimum Versus Uniform Broadcast Power Allocation

In a broadcast *ad hoc* network, information is transmitted to a set of nanotubes by distributing the limited total power among the frequency spectrum. Observing the significant SNR

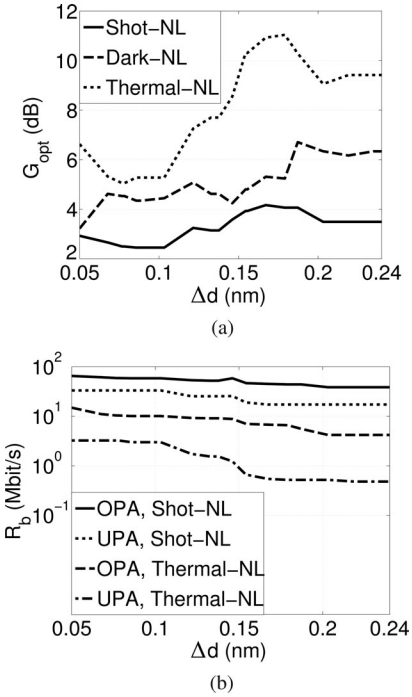

Fig. 9. (a) $G_{\rm opt}$ versus Δd for various NL cases. (b) R_b versus Δd for shot- and thermal-NL cases for OPA and UPA.

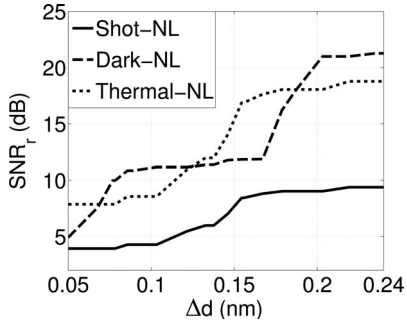

Fig. 10. SNR_r versus Δd for UPA.

difference among tubes, optimization is substantially important for nanoscale optical communication networks. The broadcast power allocation problem could be significantly important in future nanotechnology applications with limited transmitter power and distributed nanodevices, where it is difficult to interact with single devices [44].

A fair comparison between OPA and UPA is achieved by assigning power to the frequency range $(\nu_{22}^{\min} - B_l, \nu_{22}^{\max} + B_l)$, where $\nu_{22}^{\min}$ and $\nu_{22}^{\max}$ are the minimum and the maximum optical transition frequencies of the CNT network, respectively, in order to prevent consumption of power in nonabsorbing frequency bands in uniform allocation. The incident power density is set to practical level $P_{\mathrm{dens},0}$ for UPA, whereas for optimum power allocation, the total power, i.e., $P_{\mathrm{dens},0}(\nu_{22}^{\min} - B_l, \nu_{22}^{\max} + B_l)$, is distributed based on the optimization. Furthermore, $R_{\rm eq}$ is chosen freely (same along the network) by adapting to satisfy the NL conditions. BER threshold is set to 10^{-8} assuming Mb/s communication ranges and maximum achievable broadcast R_b along the network is compared for OPA and UPA, i.e., $G_{\rm opt} = R_b^{\rm opt}/R_b^{\rm uni}$. The rate of the worst performance tube determines the global rate of the network, i.e., R_b. As diameter variation of the network, i.e., Δd, increases, the gain increases in an oscillating manner as shown in Fig. 9(a), showing that as the difference among the tubes increases, the optimization brings better improvements between $\approx$2 and 11 dB for various NL cases.

Furthermore, maximum broadcast R_b at a BER of 10^{-8} is shown in Fig. 9(b). All the rates are decreased as Δd increases due to the significant decrease in $\mathrm{SNR}_{\min}$ as the smaller diameter tubes (for shot- and thermal-NL case) are encountered. However, optimization gives significant improvements, where shot-NL case performs better than thermal-NL case, giving the highest broadcast R_b but the worst gain. It is possible to increase the data rate of the worst receiver in the network by tens of Mb/s by using optimization as shown in 9(b) for shot-NL case. These are the theoretical results which could be developed and modified theoretically with future experimental results.

1) Analysis of NL Gain Behaviors: The gain behavior of NL cases for various diameter sets can be explained as the following. Since SNR $\propto I_p$ for shot-NL case, SNR $\propto I_p^2 R_{\rm eq}$ and $R_{\rm eq} = 0.1 \times \max\left(4\kappa T/(2q\mathbf{I}_p^{\rm opt})\right)$ for thermal-NL case, SNR $\propto I_p^2 e^{15.78/d}$ for dark-NL case, where $\mathbf{I}_p$ is the photocurrent vector of the tubes, if R_b is set to the same value for both OPA and UPA, the gain becomes the ratio of SNR values of the worst performance tubes for OPA and UPA and can be expressed as the following:

$$G_{\rm opt}^{\rm shot} \propto \frac{\min\left(\mathbf{I}_p^{\rm opt}\right)}{\min\left(\mathbf{I}_p^{\rm uni}\right)} \tag{20}$$

$$G_{\rm opt}^{\rm therm} \propto \frac{\min\left(\mathbf{I}_p^{\rm opt}\right)}{\min\left(\mathbf{I}_p^{\rm uni}\right)} \frac{\max\left(\mathbf{I}_p^{\rm uni}\right)/\min\left(\mathbf{I}_p^{\rm uni}\right)}{\max\left(\mathbf{I}_p^{\rm opt}\right)/\min\left(\mathbf{I}_p^{\rm opt}\right)} \tag{21}$$

$$G_{\rm opt}^{\rm dark} \propto \frac{\min\left((\mathbf{I}_p^{\rm opt})^2 \otimes \mathbf{e}\right)}{\min\left((\mathbf{I}_p^{\rm uni})^2 \otimes \mathbf{e}\right)} \tag{22}$$

where $\mathbf{e} = [e^{15.78/d_1} \ldots e^{15.78/d_N}]$, and $\otimes$ and $()^2$ denote the element-wise product and square power, respectively.

In comparison with thermal- and shot-NL cases, it is observed that their optimized power allocations are the same due to the proportionality $\gamma_t(d_t) \propto \gamma_s^2(d_t)$ which can be derived from (6)–(8) and (10). This leads to the same ratio of $\min\left(\mathbf{I}_p^{\rm opt}\right)/\min\left(\mathbf{I}_p^{\rm uni}\right)$. Furthermore, since optimum power allocation lowers $\max\left(\mathbf{I}_p^{\rm opt}\right)/\min\left(\mathbf{I}_p^{\rm opt}\right)$ and $\max\left(\mathbf{I}_p^{\rm uni}\right)/\min\left(\mathbf{I}_p^{\rm uni}\right) \propto \mathrm{SNR}_r$ gets larger as Δd increases in UPA as seen in Fig. 10, thermal-NL gain is bigger than shot-NL gain and gets larger as Δd increases based on (21) and as observed in Fig. 9(a). On the other hand, the behavior of the optimization gain for dark-NL case obeys the proportionality defined in (22), where the diameter of the worst performance tubes changes the gain in an exponential manner. Moreover, as the diameter variation is increased, the SNR ratio between the worst and best performance tubes increases drastically as shown in Fig. 10. Since, the effect of diameter on SNR is much more in

dark- and thermal-NL cases as shown in Fig. 7(a), SNR_r ratio obeys the same rule such that shot-NL case has a smaller SNR_r ratio than dark- and thermal-NL cases.

VIII. Conclusion

In this paper, CNT nanoscale optical network architecture based on M-SWNT-M photodiodes is presented and analyzed in terms of SNR, BER, and R_b. Transmitter power allocation optimization problem is defined and solved for the broadcast network with small diameter nanotubes. The receivers are theoretically modeled emphasizing the diameter dependence in terms of photocurrent and noise for shot-, dark-, and thermal-NL cases. Information broadcast to multiuser optical CNT receiver network is presented and maximizing the minimum SNR is modeled as an NP-hard max–min quadratic problem in a network of specific diameter range for thermal- and dark-NL cases and as an LP problem for shot-NL case. SDP relaxation solution is presented within a BB framework. The performance metrics are analyzed for UPA and IM/DD nonreturn-to-zero ON–OFF keying modulation for practical transmission powers. Optimum power allocation results in significant performance improvement compared with UPA in terms of SNR gain and maximum R_b showing an increasing trend with increasing diameter range. The theoretical receiver model is compared with existing experimental results using parameter fitting. Data rates reaching hundreds of Mb/s are achievable with very low BERs. Thermal-NL case gives the highest gain and shot-NL case gives the highest data rate.

References

[1] B. Atakan and O. Akan, "Carbon nanotube-based nanoscale ad hoc networks," *IEEE Commun. Mag.*, vol. 48, no. 6, pp. 129–135, Jun. 2010.

[2] A. Jorio, G. Dresselhaus, and M. Dresselhaus, *Carbon Nanotubes: Advanced Topics in the Synthesis, Structure, Properties and Applications*. Berlin, Germany: Springer-Verlag, 2008.

[3] M. Freitag, Y. Martin, J. Misewich, R. Martel, and P. Avouris, "Photoconductivity of single carbon nanotubes," *Nano Lett.*, vol. 3, pp. 1067–1071, Jun. 2003.

[4] X. Qiu, M. Freitag, V. Perebeinos, and P. Avouris, "Photoconductivity spectra of single-carbon nanotubes: Implications on the nature of their excited states," *Nano Lett.*, vol. 5, no. 4, pp. 749–752, Mar. 2005.

[5] J. Guo, M. Alam, and Y. Yoon, "Theoretical investigation on photoconductivity of single intrinsic carbon nanotubes," *Appl. Phys. Lett.*, vol. 88, pp. 133111-1–133111-3, Mar. 2006.

[6] O. Yutaka, S. Kishimoto, and T. Mizutani, "Photoresponse of carbon nanotube field-effect transistors," *Jpn. J. Appl. Phys.*, vol. 44, pp. 1592–1595, Apr. 2005.

[7] M. Pourfath, H. Kosina, and S. Selberherr, "Reduction of the dark-current in carbon nanotube photo-detectors," in *Proc. 38th Eur. Solid-State Device Res. Conf.*, Edinburgh, U.K., Sep. 2008, pp. 214–217.

[8] H. Chen, N. Xi, K. Lai, C. Fung, and R. Yang, "CNT infrared detectors using Schottky barriers and p-n junctions based FETs," in *Proc. IEEE Nanotechnol. Mater. Devices Conf.*, Traverse City, MI, Jun. 2009, pp. 91–95.

[9] L. Chen, N. Xi, H. Chen, and K. Lai, "Development of infrared detectors using single carbon-nanotube-based field-effect transistors," *IEEE Trans. Nanotechnol.*, vol. 9, no. 5, pp. 582–589, Sep. 2010.

[10] C. Chen, W. Zhang, E. Kong, and Y. Zhang, "Carbon nanotube photovoltaic device with asymmetrical contacts," *Appl. Phys. Lett.*, vol. 94, no. 26, pp. 263501-1–263501-3, Jun. 2009.

[11] D. Stewart and F. Leonard, "Energy conversion efficiency in nanotube optoelectronics," *Nano Lett.*, vol. 5, no. 2, pp. 219–222, Jan. 2005.

[12] A. Malapanis, D. Jones, E. Comfort, and J. Lee, "Measuring carbon nanotube band gaps through leakage current and excitonic transitions of nanotube diodes," *Nano Lett.*, vol. 11, pp. 1946–1951, Apr. 2011.

[13] J. Lee, "Band-gap renormalization in carbon nanotubes: Origin of the ideal diode behavior in carbon nanotube p-n structures," *Phys. Rev. B*, vol. 75, no. 7, pp. 075409-1–075409-5, Feb. 2007.

[14] S. Wang, L. Zhang, Z. Zhang, L. Ding, Q. Zeng *et al.*, "Photovoltaic effects in asymmetrically contacted CNT barrier-free bipolar diode," *J. Phys. Chem. C*, vol. 113, no. 17, pp. 6891–6893, Apr. 2009.

[15] C. Chen and Y. Zhang, *Nanowelded Carbon Nanotubes: From Field-Effect Transistors to Solar Microcells*. Berlin, Germany: Springer-Verlag, 2009.

[16] H. Li, W. Loke, Q. Zhang, and S. Yoon, "Physical device modeling of carbon nanotube/GaAs photovoltaic cells," *Appl. Phys. Lett.*, vol. 96, pp. 043501-1–043501-3, Jan. 2010.

[17] C. Chen, L. Yang, Y. Lu, G. Xiao, and Y. Zhang, "Assessment of optical absorption in carbon nanotube photovoltaic device by electromagnetic theory," *IEEE Trans. Nanotechnol.*, vol. 8, no. 3, pp. 303–314, May 2009.

[18] L. Carloni, P. Pande, and Y. Xie, "Networks-on-chip in emerging interconnect paradigms: Advantages and challenges," in *Proc. ACM/IEEE Int. Symp. Networks-on-Chip (NOCS)*, San Diego, CA, May 2009, pp. 93–102.

[19] A. Nojeh, P. Pande, A. Ganguly, S. Sheikhaei, B. Belzer, and A. Ivanov, "Reliability of wireless on-chip interconnects based on carbon nanotube antennas," in *Proc. IEEE 14th Int. Mixed-Signals, Sens., Syst. Test Workshop*, Jun. 2008, pp. 1–6.

[20] A. Nojeh and A. Ivanov, "Wireless interconnect and the potential for carbon nanotubes," *IEEE Design Test Comput.*, vol. 27, no. 4, pp. 44–53, Jul./Aug. 2010.

[21] A. Ganguly, K. Chang, S. Deb, P. Pande, B. Belzer, and C. Teuscher, "Scalable hybrid wireless Network-on-Chip architectures for multi-core systems," *IEEE Trans. Comput.*, vol. 60, no. 10, pp. 1485–1502, Oct. 2011.

[22] M. Islam and V. Logeeswaran, "Nanoscale materials and devices for future communication networks," *IEEE Commun. Mag.*, vol. 48, no. 6, pp. 112–120, Jun. 2010.

[23] J. Rockway, J. Rockway, and J. Rockway, "Signal-to-noise ratio between coupled carbon nanotube dipole antennas," in *Proc. Int. Symp. IEEE Antennas Propag. Soc.*, San Diego, CA, Jul. 2008, pp. 1–4.

[24] J. Kahn and J. Barry, "Wireless infrared communications," *Proc. IEEE*, vol. 85, no. 2, pp. 265–298, Feb. 1997.

[25] H. Manohara, E. Wong, E. Schlecht, B. Hunt, and P. Siegel, "Carbon nanotube Schottky diodes using Ti-Schottky and Pt-Ohmic contacts for high frequency applications," *Nano Lett.*, vol. 5, pp. 1469–1474, May 2005.

[26] S. Lim, J. Jang, D. Bae, G. Han, S. Lee, I.-S. Yeo, and Y. H. Lee, "Contact resistance between metal and carbon nanotube interconnects: Effect of work function and wettability," *Appl. Phys. Lett.*, vol. 95, pp. 264103-1–264103-3, Dec. 2009.

[27] P. Burke, "AC performance of nanoelectronics: Towards a ballistic THz nanotube transistor," *Solid-State Electron.*, vol. 48, pp. 1981–1986, Oct.–Dec. 2004.

[28] C. Lu, L. An, Q. Fu, J. Liu, H. Zhang, and J. Murduck, "Schottky diodes from asymmetric metal-nanotube contacts," *Appl. Phys. Lett.*, vol. 88, pp. 133501-1–133501-3, Mar. 2006.

[29] P. Avouris, M. Freitag, and V. Perebeinos, "Carbon-nanotube photonics and optoelectronics," *Nat. Photon.*, vol. 2, no. 6, pp. 341–350, Jun. 2008.

[30] Z. Luo, L. Pfefferle, G. Haller, and F. Papadimitrakopoulos, "(n, m) abundance evaluation of single-walled carbon nanotubes by fluorescence and absorption spectroscopy," *J. Amer. Chem. Soc.*, vol. 128, no. 48, pp. 15511–15516, Nov. 2006.

[31] V. Popov, L. Henrard, and P. Lambin, "Electron-phonon and electron-photon interactions and resonant Raman scattering from the radial-breathing mode of single-walled carbon nanotubes," *Phys. Rev. B*, vol. 72, no. 3, pp. 035436-1–035436-10, Jul. 2005.

[32] S. Reich, C. Thomsen, and J. Maultzsch, *Carbon Nanotubes: Basic Concepts and Physical Properties*. New York: Wiley-VCH, 2004.

[33] S. Jhang, S. Lee, D. Lee, E. Campbell, S. Roth, and Y. Park, "Random telegraph noise in individual single-walled carbon nanotubes," in *Proc. Mater. Res. Soc. Symp.*, Warrendale, Marshall, PA, 2004, vol. 858, pp. 185–190.

[34] C. Bena, "Effects of decoherence on the shot noise in carbon nanotubes," *Phys. Rev. B*, vol. 81, no. 3, pp. 033404-1–033404-3, Jan. 2010.

[35] J. Zhang, N. Xi, H. Chen, K. Lai, G. Li, and U. Wejinya, "Design, manufacturing, and testing of single-carbon-nanotube-based infrared sensors," *IEEE Trans. Nanotechnol.*, vol. 8, no. 2, pp. 245–251, Mar. 2009.
[36] F. Xia, T. Mueller, Y. Lin, A. Valdes-Garcia, and P. Avouris, "Ultrafast graphene photodetector," *Nat. Nanotechnol.*, vol. 4, pp. 839–843, Oct. 2009.
[37] T. Mueller, M. Kinoshita, M. Steiner, V. Perebeinos, A. A. Bol, D. B. Farmer, and P. Avouris, "Efficient narrow-band light emission from a single carbon nanotube p–n diode," *Nat. Nanotechnol.*, vol. 5, no. 1, pp. 27–31, Nov. 2009.
[38] B. Ellis, M. A. Mayer, G. Shambat, T. Sarmiento, J. Harris, E. E. Haller, and J. Vučković, "Ultralow-threshold electrically pumped quantum-dot photonic-crystal nanocavity laser," *Nat. Photon.*, vol. 5, pp. 297–300, Apr. 2011.
[39] S. Choi and K. Sarabandi, "Performance assessment of bundled carbon nanotube for antenna applications at terahertz frequencies and higher," *IEEE Trans. Antennas Propag.*, vol. 59, no. 3, pp. 802–809, Mar. 2011.
[40] P. J. Burke, S. Li, and Z. Yu, "Quantitative theory of nanowire and nanotube antenna performance," *IEEE Trans. Nanotechnol.*, vol. 5, no. 4, pp. 314–334, Jul. 2006.
[41] F. K. Tittel, D. Richter, and A. Fried, "Mid-infrared laser applications in spectroscopy," *Top. Appl. Phys.*, vol. 89, pp. 445–516, 2003.
[42] M. A. Ummy, N. Madamopoulos, A. Joyo, M. Kouar, and R. Dorsinville, "Tunable multi-wavelength SOA based linear cavity dual-output port fiber laser using Lyot-Sagnac loop mirror," *Opt. Express*, vol. 19, pp. 3202–3211, Feb. 2011.
[43] S. Magazine, "Modeling SWCNT bandgap and effective mass variation using a Monte Carlo approach," *IEEE Trans. Nanotechnol.*, vol. 9, no. 2, pp. 184–193, Mar. 2010.
[44] I. Akyildiz, F. Brunetti, and C. Blázquez, "Nanonetworks: A new communication paradigm," *Comput. Netw.*, vol. 52, pp. 2260–2279, Aug. 2008.
[45] N. Sidiropoulos, T. Davidson, and Z. Luo, "Transmit beamforming for physical-layer multicasting," *IEEE Trans. Signal Process.*, vol. 54, no. 6, pp. 2239–2251, Jun. 2006.
[46] M. Jordan, M. Senst, G. Ascheid, and H. Meyr, "Long-term beamforming in single frequency networks using semidefinite relaxation," in *Proc. IEEE VTC 2008-Spring*, Marina Bay, Singapore, May 2008, pp. 275–279.
[47] Y. Zhang, "User's guide to LIPSOL: Linear programming interior point solver v0.4," *Optim. Method Softw.*, vol. 11, pp. 385–396, 1999.
[48] I. Nowak, "A new semidefinite programming bound for indefinite quadratic forms over a simplex," *J. Global Optim.*, vol. 14, pp. 357–364, Jun. 1999.
[49] J. Sturm, "Using SeDuMi 1.02, a Matlab toolbox for optimization over symmetric cones," *Optim. Method Softw.*, vol. 11, pp. 625–653, 1999.
[50] M. Grant and S. Boyd. (2011, Apr.). "CVX: Matlab software for disciplined convex programming, version 1.21," [Online]. Available: http://cvxr.com/cvx.
[51] C. A. Floudas, *Nonlinear and Mixed-Integer Optimization*. London, U.K.: Oxford Univ. Press, 1995.
[52] L. Prechtel, L. Song, S. Manus, D. Schuh, W. Wegscheider, and A. Holleitner, "Time-resolved picosecond photocurrents in contacted carbon nanotubes," *Nano Lett.*, vol. 11, pp. 269–272, Jan. 2011.
[53] J. Proakis and M. Salehi, *Digital Communications*. New York: McGraw-Hill, 1995.

Burhan Gulbahar received the B.S. and M.S. degrees in electrical and electronics engineering from Bilkent University, Ankara, Turkey, in 1999 and 2002, respectively. He is currently working toward the Ph.D. degree in the Department of Electrical and Computer Engineering, Koc University, Istanbul, Turkey.

He is also a Research Assistant at Next-generation and Wireless Communications Laboratory. His research interests include quantum communications, nanoscale optical communications, carbon nanotube communication networks, underwater communication networks, cognitive radio networks, and wireless sensor networks.

Ozgur B. Akan (M'00–SM'07) received the B.S. and M.S. degrees in electrical and electronics engineering from Bilkent University and Middle East Technical University, Ankara, Turkey, in 1999 and 2001, respectively, and the Ph.D. degree in electrical and computer engineering from the Broadband and Wireless Networking Laboratory, School of Electrical and Computer Engineering, Georgia Institute of Technology, Atlanta, in 2004.

He is currently an Associate Professor with the Department of Electrical and Electronics Engineering, and the Director of Next-generation and Wireless Communications Laboratory, Koc University, Istanbul, Turkey. His current research interests include wireless communications, acoustic communications, nanocommunications, and information theory.

Dr. Akan is an Associate Editor for the IEEE TRANSACTIONS ON VEHICULAR TECHNOLOGY, the *International Journal of Communication Systems* (Wiley), the *European Transactions on Telecommunications*, and the *Nano Communication Networks Journal* (Elsevier). He served as an Editor for *ACM/Springer Wireless Networks (WINET) Journal* from 2004 to 2010, as an Area Editor for *AD HOC Networks Journal* (Elsevier) from 2004 to 2008, as a Guest Editor for several special issues, as the TPC Co-Chair for the 13th ACM International Conference on Modeling, Analysis and Simulation of Wireless and Mobile Systems (ACM MSWiM 2010), the General Co-Chair for the Third International Conference on Bio-Inspired Models of Network, Information, and Computing Systems (ICST/IEEE BIONETICS 2008), the European Vice Chair for the Second International Conference on Nano-Networks (ICST/ACM Nano-Net 2007), an International Vice Chair for the IEEE INFOCOM 2006, and in organizing committees and technical program committees of many other international conferences. He is the Vice President of the IEEE Communications Society—Turkey Section. He is a Senior Member of the IEEE Communications Society (COMSOC), and a member of ACM. He is a COMSOC Distinguished Lecturer (2011–2012). He received the IEEE COMSOC Outstanding Young Researcher Award for EMEA Region 2010 (as runner-up), the IBM Faculty Award twice in 2010 and 2008, and the Turkish Academy of Sciences Distinguished Young Scientist Award 2008 (TUBA-GEBIP).